

Tetragonal domain structure and magnetoresistance of $\text{La}_{1-x}\text{Sr}_x\text{CoO}_3$

Z. L. Wang

School of Materials Science and Engineering, Georgia Institute of Technology, Atlanta, Georgia 30332-0245

Jiming Zhang*

Advanced Technology Materials, Inc., 7 Commerce Drive, Danbury, Connecticut 06810

(Received 11 December 1995; revised manuscript received 11 March 1996)

$\text{La}_{1-x}\text{Sr}_x\text{CoO}_3$ (LSCO) has recently been found to exhibit large magnetoresistance (MR) effect. In this paper, microstructures of LSCO thin films, which may provide important clues for understanding the unusual MR characteristics in these intrinsic magnetic oxides, were determined by transmission electron microscopy. An ordered, anisotropic perovskite-type structure *n*-LSCO was observed and its atomic model was determined. The ordered structure has a tetragonal cell with a La-Co-Sr-Co-[001] layered atom distribution along the *c* axis. This structure is intrinsic for the LSCO system and is resulted directly from the lattice substitution between La and Sr. The entire film is composed of [001], [010], and [100] anisotropic domains of sizes in the order of 30–200 nm. Microstructures of (011)- and (001)-type domain boundaries were determined. Although *n*- $\text{La}_{0.5}\text{Sr}_{0.5}\text{CoO}_3$ is the dominant structure, a tetragonal phase *n*- $\text{La}_{0.33}\text{Sr}_{0.67}\text{CoO}_3$ has also been identified, which is produced by both the lattice substitution between La and Sr and the variation of local chemical composition. These structures could play a key role in determining the MR properties of the materials which are believed due to the intrinsic coupled spin scattering of Co atoms in different atomic layers. [S0163-1829(96)09726-3]

I. INTRODUCTION

Recent research has shown thousandfold improvements in magnetoresistance performance with a type of intrinsic magnetic oxides, $(\text{La},A)\text{MnO}_3$ ($A = \text{Ca, Sr, or Ba}$).^{1–5} These type of materials are referred to as *colossal magnetoresistive* (CMR) oxides because of their huge magnetoresistance (MR) ratio. CMR's were observed in a group of manganese oxides. A very large magnetoresistance ratio ($\Delta R/R(H) > -100\,000\%$) was reported in epitaxially grown $\text{La}_{0.67}\text{Ca}_{0.33}\text{MnO}_3$ (LCMO) films.¹ More recently, a large MR ratio has been reported in another group of intrinsic magnetoresistive oxides, $(\text{La},A)\text{CoO}_3$ ($A = \text{Ca, Sr, or Ba}$).⁶ These CMR oxides offer exciting possibilities for improved magnetic sensors, magnetoresistive read heads, and magnetoresistive random access memory. The potential for integration with silicon technology makes these oxides particularly attractive for applications in advanced technologies. Magnetic sensors, as one of the potential applications of CMR's, play important roles in many commercial markets and scientific research activities.

$\text{La}_{1-x}\text{Sr}_x\text{CoO}_3$ (LSCO) thin films are also conductive,⁷ and they can be used as electrodes for fuel cells and nonvolatile memories. The LSCO electrode is particularly interesting for nonvolatile memories because it exhibits isotropic, low electric resistivity and good lattice and structural compatibility with the ferroelectric Pb-Zr-Ti-O films.⁸ Epitaxial LSCO films have been grown on both sides of Pb-Zr-Ti-O ferroelectric film to make ferroelectric capacitors,^{9,10} which exhibit superior fatigue and retention characteristics to capacitors using conventional Pt electrodes. For LSCO, the variation of the chemical composition has a great impact on the quality and physical properties of the film, since the highest electric conductivity is found at $x=0.5$. The quality of

the grown LSCO film is largely influenced by the lattice and structure compatibility of the substrate. It is thus essential to examine the microstructure of the grown film and the interface between the substrate and the film.

In this paper, microstructures of LSCO thin films grown on $\text{LaAlO}_3(001)$ (LAO) by a liquid source metal-organic chemical-vapor deposition (MOCVD) technique are analyzed using high-resolution transmission electron microscopy (HRTEM). An ordered, anisotropic perovskite-type (or tetragonal) structure, denoted as *n*- $\text{La}_{0.5}\text{Sr}_{0.5}\text{CoO}_3$, is identified and its structural model is determined. The grown film exhibits domain structure and the structural anisotropic direction (or *c* axis) changes from domain to domain. A type of structure denoted as *n*- $\text{La}_{0.33}\text{Sr}_{0.67}\text{CoO}_3$ is also observed and its atomic structure is determined. These structures are formed owing to site substitution between La and Sr and the change of local chemical composition. Finally, the LSCO/LAO and domain interfacial structures have been examined, and the results indicate that the LSCO film starts to grow from a Co-O layer. The roles played by the observed microstructures in determination of the MR ratio are discussed.

II. EXPERIMENTAL METHOD

The LSCO films were grown on polished $\text{LaAlO}_3(001)$ substrate by a liquid source MOCVD technique. Details of the liquid source MOCVD technique have been reported elsewhere.^{11,12} Briefly, the requisite β -diketonate complexes $[M(\text{thd})_n]$, thd = 2,2,6,6-tetramethyl-3,5-heptanedionate, $M = \text{La, Sr, Ca}$ were dissolved in an organic solvent and the solution was injected by a liquid pump into a heated, stainless steel vaporizer which was maintained at 220 °C during deposition. The film composition was controlled by varying the molar ratio of the organometallic complexes in the solu-

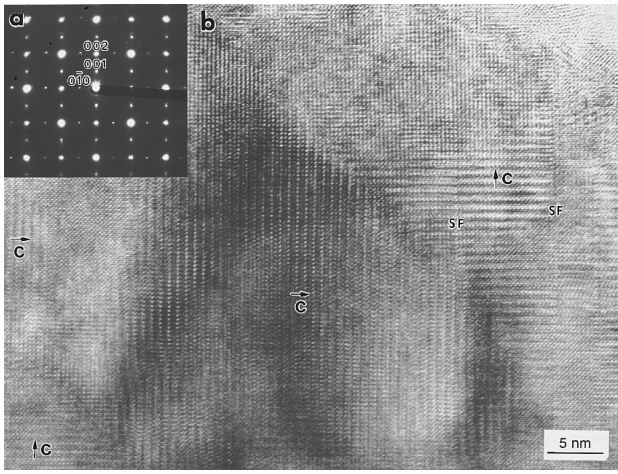


FIG. 1. (a) A [100] electron-diffraction pattern from a cross-section LSCO/LAO specimen, showing the epitaxial growth of LSCO. The (001) and (010) reflections, which should be extinct, appear in the diffraction pattern, corresponding to the formation of ordered anisotropic structure in LSCO. (b) A cross-section TEM image of LSCO showing anisotropic [001] and [010] domain structures. A few stacking faults (SF) confined in the (010) plane are also seen.

tion. The precursor vapor was carried upstream of the reactor inlet by nitrogen carrier gas (flow rate = 50–100 sccm) and the vaporization process took place on a continuous basis. The reactor pressure was maintained at 1.5–2.0 Torr. The deposition temperature was controlled at 600–700 °C. The nominal composition of the film is La:Sr:Co:O = 1:1:2:6 (or $\text{La}_{0.5}\text{Sr}_{0.5}\text{CoO}_3$).

The LaAlO_3 substrate has the distorted-perovskite structure with lattice constant $a=b=c=0.3788$ nm and $\alpha=\beta=\gamma=90.066^\circ$.¹³ The structure is referred to a face-centered-rhombohedral cell, in which the La^{+3} ion locates at (000), the Al^{+3} ion at $(\frac{1}{2}\frac{1}{2}\frac{1}{2})$, and the O^{-2} ions at the face centers $\{\frac{1}{2}\frac{1}{2}0\}$. Recently {001} surfaces of annealed LAO in air have been studied using reflection electron microscopy.^{14,15} The surface is atom flat, but exhibiting many atom-high $\langle 100 \rangle$ steps. These steps are the lowest surface energy steps.

Cross-sectional TEM specimens were prepared using the standard procedures of cutting, gluing, slicing, grinding, and ion milling. The specimen was cooled to liquid-nitrogen temperature during ion milling to avoid any structural transformation and damage. High-resolution transmission electron microscopy (HRTEM), select-area electron diffraction (SAD) and dynamical image simulations were used to determine the microstructure. HRTEM experiments were performed at 300 kV with the use of a charge-coupled device (CCD) camera for digital data recording. The recorded data can be digitally processed in order to be compared to the theoretically calculated images.

III. STRUCTURES OF LSCO FILM

The grown LSCO film is single crystalline and has an epitaxial relationship with the LAO substrate. Figure 1(a) shows an SAD pattern recorded from a cross-section sample

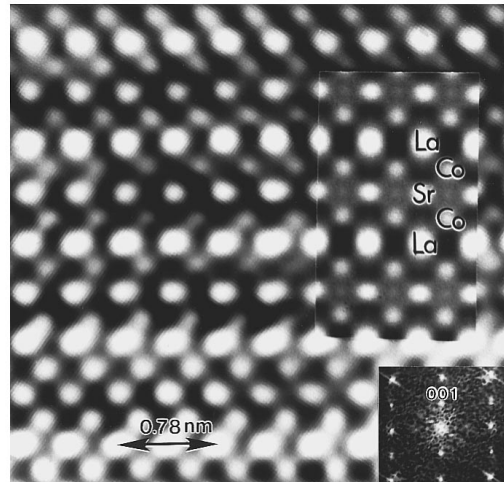


FIG. 2. An HRTEM image recorded from a region exhibiting [001] directional domain structure. A Fourier specimen of the image is shown at the low-right corner. The inset is a theoretically simulated image based on the structure model shown in Fig. 3(b) for the following parameters: electron-beam energy 300 kV, specimen thickness 3.875 nm, beam convergence 0.3 mrad, mechanical vibration of the microscope 0.03 nm, objective lens defocus 15 nm, focus spread 10 nm, objective lens spherical aberration 0.6 nm, and objective aperture radius 1.0 \AA^{-1} . The atoms show bright contrast under this defocus condition.

of LSCO/LAO. Since the lattice constant of LSCO is 0.7668 nm, twice the lattice constant of LAO being 0.7576 nm, the lattice mismatch is so small that the splitting between the reflections of LAO and those of LSCO is hardly seen in the electron-diffraction pattern. The LAO substrate and the LSCO film apparently have an epitaxial relationship of

$$(001)_{\text{LAO}} \parallel (001)_{\text{LSCO}} \text{ and } [100]_{\text{LAO}} \parallel [100]_{\text{LSCO}}$$

In addition to the allowed reflections of LSCO, a remarkable phenomenon is the presence of (001) and (010) reflections of LSCO, which should be extinct if the ideal, isotropic perovskite-type structure remains. The {001} reflections are produced by the periodic projected structure of the crystal along $\langle 001 \rangle$ with a periodicity of c , the lattice constant of the c axis.

To find the origin of the observed {001} reflections, a cross-section TEM image of the LSCO film is shown in Fig. 1(b). It is apparent that the film exhibits domain structure, and the c -axis direction changes from domain to domain. Therefore, the (001) and (010) reflections are generated from the domains exhibiting [001] and [010] anisotropic n -LSCO structure, respectively. A (011) boundary between the two [001] and [010] anisotropic n -LSCO domains is seen. The three-dimensional structure of the film is composed of domains with [001], [010], and [100] directional anisotropic n -LSCO structure.

The real-space correspondence of the {001} reflection is directly seen in the HRTEM image. Figure 2 shows a cross-section TEM image of the LSCO film, exhibiting c -axis directional, anisotropic structure of periodicity c . The domain size is approximately 50–300 nm. The Fourier transform of this image does show the (001) reflection but the (010) re-

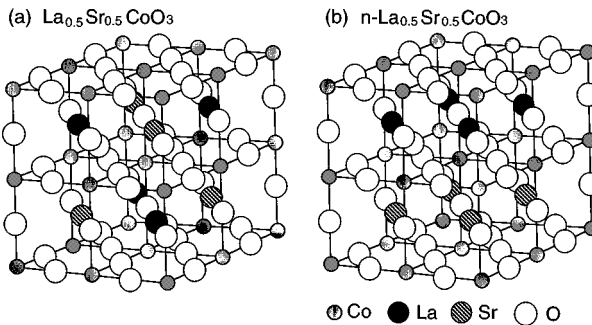


FIG. 3. Atomic models for (a) isotropic perovskite-type structure and (b) the proposed anisotropic perovskite-type *n*-LSCO structure. For clarity, these models are drawn to schematically show the atom distribution in the unit cell, and the sizes of the balls in these figures may not represent the real sizes of the cations.

flection is extinct. This observation indicates that (010) and (001) do not belong to the same family of reflections of the same crystal. For the convenience of following discussion, the observed anisotropic structure is denoted as $n\text{-La}_{0.5}\text{Sr}_{0.5}\text{CoO}_3$ (or *n*-LSCO).

In order to propose a lattice model of the newly observed anisotropic structure, the lattice model of $\text{La}_{0.5}\text{Sr}_{0.5}\text{CoO}_3$, with space group $Fm\bar{3}m$, is examined first. The ideal $\text{La}_{0.5}\text{Sr}_{0.5}\text{CoO}_3$ has the pseudocubic perovskite-type structure with lattice constant of 0.7668 nm, as shown in Fig. 3(a).^{16,17} The {001} reflections are extinct for this atomic model, and an identical structure is preserved regardless the beam direction is [100], [010], or [001]. The structure, however, does allow (001) reflection but does not allow (100) and (010) reflections. Moreover, the chemical composition of the structure must match the measured overall film composition of La:Sr:Co:O = 1:1:2:6, because *n*-LSCO is the dominant structure. With consideration of all these factors, a structural model is shown in Fig. 3(b). The model is built based on the ideal model shown in Fig. 3(a) by rearranging the Sr and La sites so that the Sr atoms located at the $z=0$ plane are entirely replaced by La and the La atoms located at $z=c/2$ plane by Sr, and the Co atom sites remain unchanged. Thus, the La and Sr atoms are distributed in different (001) atomic planes, exhibiting La-Co-Sr-Co-La-Co-Sr-Co-(001) layered structure.

In order to verify the atomic model, image simulations are performed based on the lattice model shown in Fig. 3(b), a calculated [100] image is shown in the inset of Fig. 2. The calculations were based on the dynamical electron-diffraction theory with considerations of the contrast transfer of the objective lens as well as the practical operation conditions of the electron microscope. The image contrast is approximately scaled according to the atomic number. The La atom shows the strongest intensity, the Sr atom weaker, and the Co atom the weakest. It is apparent that the simulated image shows an excellent agreement with the observed image.

Figures 4(a) and 4(c) are the dynamical calculated electron-diffraction patterns and Figs. 4(b) and 4(d) are the calculated HRTEM images based on the ideal perovskite and anisotropic perovskite-type structural models shown in Figs. 3(a) and 3(b), respectively. The (001) reflection which is extinct in Fig. 4(a) does appear in Fig. 4(c) in correspon-

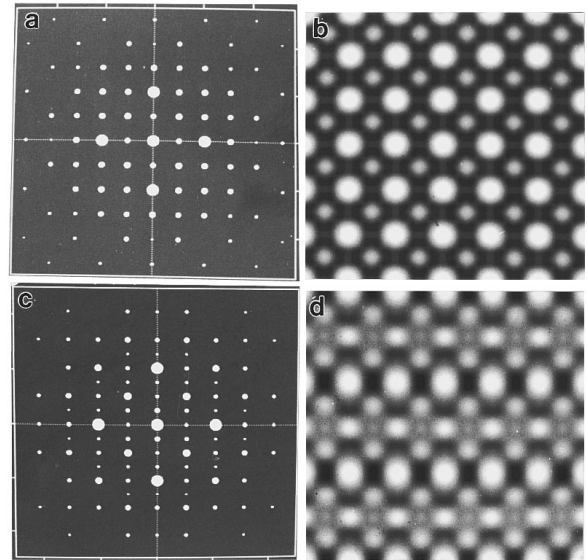


FIG. 4. Simulated (a,c) [100] electron-diffraction patterns and (b,d) corresponding lattice images for the isotropic perovskite-type structure of LSCO and anisotropic perovskite-type of *n*-LSCO shown in Figs. 3(a) and 3(b), respectively.

dence to the experimental observation. The image contrast is also very different for the two models. Thus, the ordered lattice substitution between La and Sr can be easily determined experimentally because of the large difference between the atomic numbers.

From the structure model shown in Fig. 3(b), the atom distribution along the *c* axis is not equivalent to that along the *a* axis (or *b* axis). Thus, the lengths of the *a* and *c* axes are expected to be different. In order to verify this prediction, x-ray diffraction was performed on the as-grown film and the result is shown in Fig. 5. The *n*-LSCO (001) reflection, although weak, does show up in the diffraction spectrum. It is noticed that the reflection angle of *n*-LSCO (200) is slightly less than that of *n*-LSCO (002), indicating that the

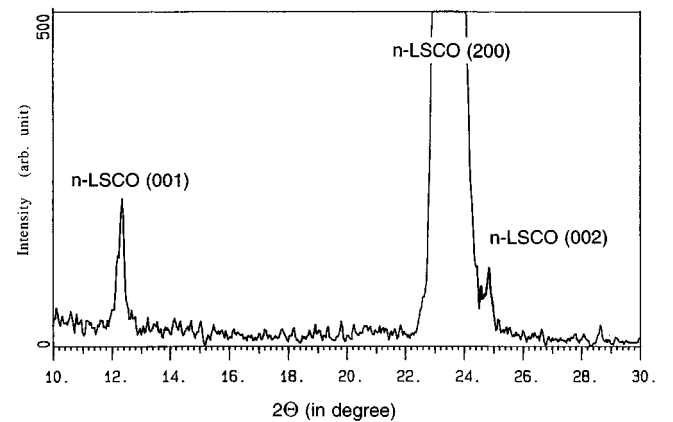


FIG. 5. X-ray-diffraction spectrum of LSCO/LAO showing the presence of (001) reflection. This result indicates that *n*-LSCO is the native structure of the as-grown LSCO film. It is important to note that the reflection angle of *n*-LSCO (200) is slightly less than that of *n*-LSCO (002), indicating that the *n*-LSCO has tetragonal structure.

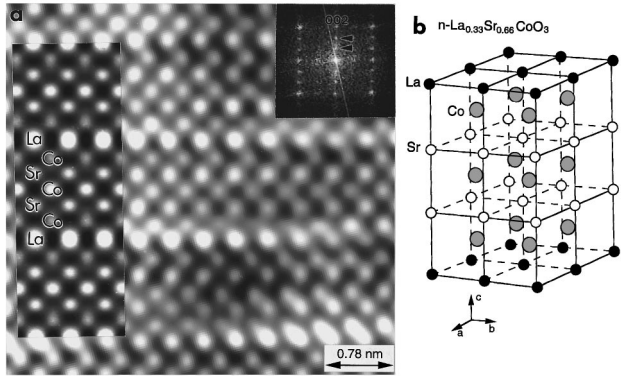


FIG. 6. (a) A high-resolution TEM image of cross-section LSCO film showing a type of [001] anisotropic structure. A Fourier spectrum of the image is also shown. (b) A schematic cation atomic model of a $\text{La}_{0.33}\text{Sr}_{0.67}\text{CoO}_3$ perovskite-type tetragonal structure, where the sizes of the balls may not represent the real sizes of the cations. A simulated HRTEM image based on this model is shown in the inset of (a).

n-LSCO has a tetragonal cell. The ratio of c/a is measured directly from the x-ray-diffraction data and the result is 0.945. More importantly, the presence of the (001) reflection in the x-ray-diffraction spectrum does indicate that the observed *n*-LSCO structure is the as-grown structure of the specimen.

Composition fluctuation in $\text{La}_{1-x}\text{Sr}_x\text{CoO}_3$ can dramatically change the local atomic structure. Figure 6(a) shows an HRTEM image of LSCO/LAO, exhibiting anisotropic structure of periodicity approximately $3/2c$ along [001], where c is the c -axis lattice constant of LSCO. The image contrast approximately characterizes the atom type of each column under particular defocus condition. The Fourier transform of the image, shown in the inset, shows the presence of (0 0 2/3) and (0 0 4/3) reflections, as indicated by arrowheads. These reflections characterize a newly ordered structure along [001]. Since the (010) reflection is absent in the Fourier spectrum, the projected structural periodicity along [010] is $a/2$.

Several factors must be considered to build an atomic model of the observed anisotropic structure. First, the periodicity of the structures is $3/2c$ along [001] and is a along [010]/[100]. Second, the total charge of the ionic structure must be zero. Since the oxygen vacancies associated with the structure is unknown, at least based on the HRTEM data, we assume that the total oxygen content is the same as that in the isotropic LSCO. Third, the concentrations of La and Sr atoms have to be complimentary in $\text{La}_{1-x}\text{Sr}_x\text{CoO}_3$, so that the atomic concentrations obey $n_{\text{La}}+n_{\text{Sr}}=1$. Finally, the site distribution of each element must approximately match the symmetry and contrast observed in the HRTEM image shown in Fig. 6(a). Based on these principles, a structure model shown in Fig. 6(b) is built, where only cations are shown for clarity. The anion distribution around each cation is assumed to be the same as that in the isotropic perovskite LSCO structure in order to preserve the charge neutrality of the entire unit cell. The ratio of the c' and a' lattice constants of this structure is $c'/a'=1.62$, which is determined from the Fourier spectrum shown in the inset of Fig. 6(a). A simulated image based on this model is shown in the inset of

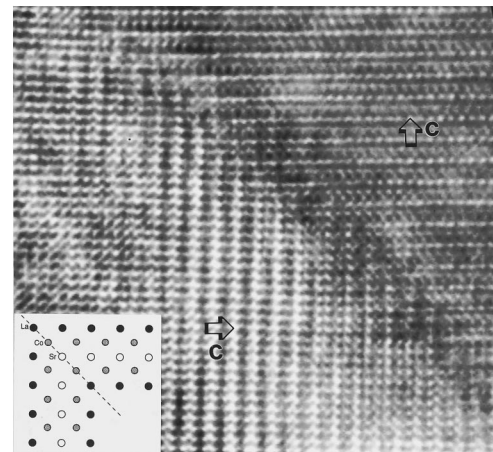


FIG. 7. A cross-section [100] HRTEM image of *n*-LSCO showing the (011)-type domain boundary. The inset is an atomic model of the domain boundary constructed using the information provided by the image and the model shown in Fig. 3(b) as well.

Fig. 6(a), which shows reasonable agreement with the observed image. The contrast of the La atoms has a good match. The contrast of Sr and Co atoms shows reasonable agreement with the observed image. In the simulated image, it is interesting to note that the contrast of the Co atoms in a unit cell is not identical because of the nonsymmetric scattering of the neighbor atoms. The first-nearest neighbors of the Co atoms located at $z=0.5$ are all Sr, but those of the Co atoms located at $z=0.167$ (or equivalently $z=0.833$) are Sr and La.

IV. DOMAIN BOUNDARIES

The tetragonal structure of *n*-LSCO can produce domain structures in the grown films. The typical domain boundaries observed in LSCO are (011) and (001). The two adjacent domains are oriented with a rotation angle of 90° . Figure 7 shows an HRTEM image of a (011)-type domain boundary. It can be seen from the image that the same type of element meets at the interface. Based on the structural model shown in Fig. 3(b), the projected atom arrangement at the boundary can be determined, as shown in the inset of Fig. 7. The dashed line indicates the (011) domain boundary. This structure model satisfies the symmetry of both domains.

The (001) domain boundary has also been observed (Fig. 8). The atom arrangement at the boundary is schematically shown in the inset of Fig. 8. The La atom at a position marked by an arrowhead is indicated in the image, showing bright contrast. No second phase is seen at the domain boundary. The domain structure is a major structural phenomenon in LSCO, but the mechanism forming the domain is not yet clear.

V. LSCO/LAO INTERFACE

Lattice mismatch at the interface is a source for creating interfacial dislocations. From the symmetry of the structure model for isotropic LSCO, two LAO unit cells tend to match an LSCO unit cell. Since the lattice constant for LAO is $d_1=0.3788$ nm, half of the lattice constant of LSCO being

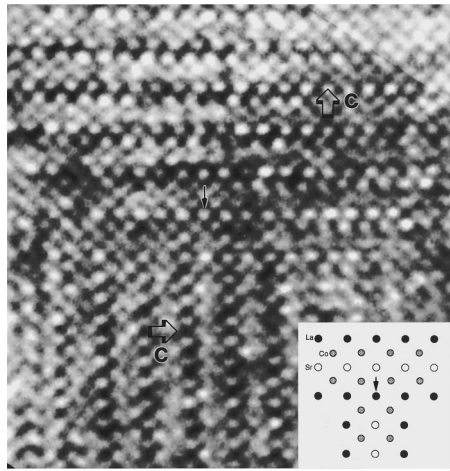


FIG. 8. A cross-section [100] HRTEM image of *n*-LSCO showing the (001)-type domain boundary. The inset is an atomic model for the domain boundary constructed using the information provided by the image and the model shown in Fig. 3(b) as well.

$d_2 = 0.385$ nm, a lattice mismatch less than 2% at the interface is expected. Figure 9 shows an HRTEM image of LSCO/LAO interface, where the dashed line indicates the last La-O layer of the LAO substrate. Recent studies have shown that the {100} surfaces of LAO are terminated entirely with either the La-O layer or the Al-O layer, but not the mixture of both.¹⁴ From the image shown in Fig. 9, the LAO substrate is terminated with the La-O layer. No interfacial reaction is seen. The LSCO film is grown coherently on the LAO lattice and the interface dislocations are rarely seen. Strain fields associated with the interface are rather weak so that the atom positions near the interface can be clearly resolved. The dark spots are the atoms because the image was recorded under the Schertzer defocus condition.¹⁸ From the symmetry of the LSCO structure, it can be concluded that the LSCO film starts to grow from a Co-O layer, as indicated. This is natural because the Al sites in LAO are equivalent to those of Co in LSCO, thus, the lattice substitution of Al by

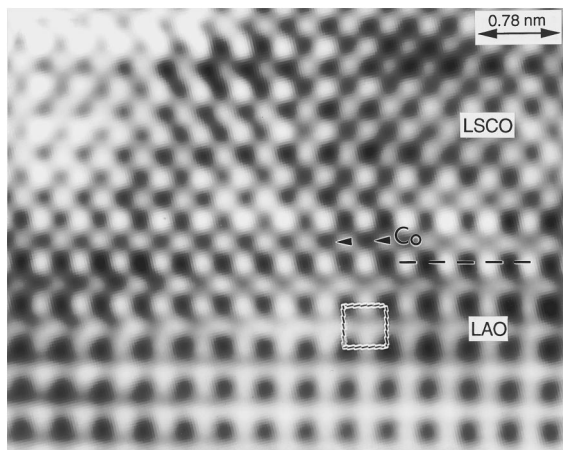


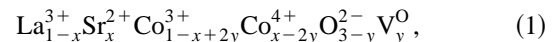
FIG. 9. A cross-section [100] HRTEM image of LSCO/LAO interface showing the nonreactive, coherent growth of LSCO. The dark spots are the projected atomic columns under Schertzer focus condition.

Co is expected, resulting in the growth of LSCO. Interface microstructure of LSCO with MgO (100) has been reported previously.²⁶

VI. DISCUSSION

A. $\text{La}_{0.5}\text{Sr}_{0.5}\text{CoO}_3$

The structure model proposed in Figs. 3(b) is based on an assumption that lattice substitution between Sr and La is permitted in LSCO for the following reasons. First, both La^{3+} and Sr^{2+} cations have the same ionic radii, thus, a site exchange will not introduce any significant lattice distortion.¹⁶ Second, the site distribution of O^{2-} anions around either La^{3+} or Sr^{2+} is equivalent, permitting lattice substitution between La^{3+} and Sr^{2+} . Third, substitution of Sr^{2+} by La^{3+} introduces a local charge compensation, but the local *p*-type charge carrier is balanced by the conversion of Co^{4+} into Co^{3+} . Finally, the loss of local charge due to substitution of La^{3+} by Sr^{2+} is balanced by creating oxygen vacancies as well as the conversion of Co^{3+} into Co^{4+} , as proposed by Jonker and van Santen.¹⁹ The ionic structure of LSCO is



where V_y^{O} stands for the ratio of oxygen vacancies.^{16,19,20} This formula has been applied to interpreting the electric conductivity of LSCO as a function of Sr content.^{16,19} If there is no oxygen vacancy ($y=0$), the ionic state of LSCO is $\text{La}_{1-x}^{\text{3+}}\text{Sr}_x^{\text{2+}}\text{Co}_{1-x}^{\text{3+}}\text{Co}_x^{\text{4+}}\text{O}_3^{\text{2-}}$ or equivalently $[\text{La}^{\text{3+}}\text{Co}^{\text{3+}}]_{1-x} [\text{Sr}^{\text{2+}}\text{Co}^{\text{4+}}]_x \text{O}_3^{\text{2-}}$. For $x=0.5$, the ionic state of $\text{La}_{0.5}\text{Sr}_{0.5}\text{CoO}_3$ is $[\text{La}^{\text{3+}}\text{Co}^{\text{3+}}]_{0.5} [\text{Sr}^{\text{2+}}\text{Co}^{\text{4+}}]_{0.5} \text{O}_3^{\text{2-}}$. Therefore, the lattice substitution between La and Sr is possible because of the double valence states of Co (Co^{4+} and Co^{3+}). The conductivity of LSCO is due to the transfer of electrons between Co^{3+} and Co^{4+} ,²¹ and the transfer probability of the electrons is directly related to the angle Θ_{ij} between the spins of the ions^{22–24}

$$t_{ij} = b_{ij} \cos(\Theta_{ij}/2), \quad (2)$$

where b_{ij} is a constant depending on the isolation between the ions. Structural evolution introduces changes not only in the intrinsic isolation but also in the spin-coupling between Co ions. The angle between the spins of two ions will be changed under an external magnetic field. Thus, the electron transfer probability across the ions (or equivalently the conductivity) is affected according to Eq. (2), possibly leading to the observed CMR effect.

However, the CMR ratio may be critically affected by the domain structure. In fact, the MR ratio of LSCO is much lower than that of LCMO, and the LCMO film does not exhibit domain structure.²⁵ However, LSCO films are composed of domains exhibiting [100], [010], and [001] directional anisotropic structure. Although each domain may exhibit high MR ratio due to the tetragonal structure, the overall MR ratio of the entire film may not be high because the small size anisotropic domains are distributed with equal probability along the *a* or *b* axis, the spatial average may reduce the MR ratio.

B. $\text{La}_{0.67}\text{Sr}_{0.33}\text{CoO}_3$

From the model shown in Fig. 6(b) the structure is formed not only due to lattice substitution between La and Sr, but also composition variation so that $\text{La}:\text{Sr}:\text{Co}=1:2:3$. Based on the same assumption that the lattice substitution between La^{3+} and Sr^{2+} is compensated by the valence state conversion between Co^{3+} and Co^{4+} , for $x=0.67$, the ionic structure of $\text{La}_{0.33}\text{Sr}_{0.67}\text{CoO}_3$ is thus $\text{La}_{0.33}^{3+}\text{Sr}_{0.67}^{2+}\text{Co}_{0.33}^{3+}\text{Co}_{0.67}^{4+}\text{O}_{2-}^2$ or equivalently $[\text{La}^{3+}\text{Co}^{3+}]_{0.33} [\text{Sr}^{2+}\text{Co}^{4+}]_{0.67}\text{O}_3^{2-}$. Therefore, the La^{3+} ions are packed with Co^{3+} ions and Sr^{2+} with Co^{4+} . Thus, the observed phase is stable.

VII. CONCLUSION

In conclusion, a MOCVD grown LSCO film is dominated by an ordered, anisotropic perovskite-type structure, $n\text{-La}_{0.5}\text{Sr}_{0.5}\text{CoO}_3$. This structure is intrinsic and is the direct result of lattice substitution between La and Sr. The atomic model of the structure is determined. The entire LSCO film is composed of [001], [010], and [100] directional anisotropic structure domains of sizes in the order of 30–200 nm.

Since n -LSCO is the most popular structure in LSCO, the physical properties of the grown film is determined by the size of the domains and the anisotropy of the tetragonal domains. The CMR effect is believed due to the intrinsic coupled spin scattering of Co atoms in different atomic layers. Therefore, the newly observed tetragonal domain structure may provide important clues for understanding the low MR ratio of LSCO in comparison to that of LCMO.

A structure denoted as $n\text{-La}_{0.33}\text{Sr}_{0.67}\text{CoO}_3$, has been observed and its atomic structural model is determined. It must be pointed out that this structure is the minor phase. The structure is the result of lattice substitution between La and Sr as well as the fluctuation of the local chemical composition. The lattice substitution between La^{3+} and Sr^{2+} is possible because of the conversion of Co valence state between Co^{3+} and Co^{4+} .

The LSCO/LAO interface has a small lattice mismatch, resulting in almost perfect, coherent growth of LSCO. The LAO [001] substrate tends to terminate with a La-O layer and a LSCO film starts to grow from a Co-O layer.

^{*}Current address: Motorola, Inc., 3501 Ed Bluestein Boulevard, MD: K-10 Austin, Texas 78721.

¹K. Chahara, T. Ohno, M. Kasai, and Y. Kozono, *Appl. Phys. Lett.* **63**, 1990 (1993).

²R. von Helmolt, J. Wecker, B. Holzapfel, L. Schultz, and K. Samwer, *Phys. Rev. Lett.* **71**, 2331 (1994).

³S. Jin, T. H. Tiefel, M. McCormack, R. A. Fastnacht, R. Ramech, and L. H. Chen, *Science* **264**, 413 (1994).

⁴H. L. Ju, C. Kwon, R. L. Greenne, and T. Venkatesan, *Appl. Phys. Lett.* **65**, 2108 (1994).

⁵Y. Q. Li, J. Zhang, S. Pombrik, S. DiMascio, W. Stevens, Y. F. Yan, and N. P. Ong, *J. Mater. Res.* (to be published).

⁶G. Briceno, X. -D. Xiang, H. Chang, X. Sun, and P. G. Schultz, *Science* **270**, 273 (1995).

⁷P. M. Raccah and J. B. Goodenough, *J. Appl. Phys.* **39**, 1209 (1968); *Phys. Rev.* **155**, 932 (1967).

⁸G. B. Eon, R. J. Cava, R. M. Fleming, J. M. Philips, R. B. Van Dover, J. H. Marshall, J. W. P. Hsu, J. J. Krajewski, and W. F. Peck, *Science* **258**, 1766 (1992); R. Ramesh, T. Sands, and V. G. Keramidas, *J. Electron. Mater.* **23**, 19 (1994).

⁹R. Ramesh, H. Gilchrist, T. Sands, V. G. Keramidas, R. Haakenaasen, and D. K. Fork, *Appl. Phys. Lett.* **63**, 3592 (1993).

¹⁰R. Dat, D. J. Lichtenwalner, O. Auciello, and A. I. Kingon, *Appl. Phys. Lett.* **64**, 2673 (1994).

¹¹J. Zhang, G. J. Cui, D. Gordon, P. Van Buskirk, and J. Steinbeck, in *Ferroelectric Thin Films III*, edited by E. R. Myers, B. A.

Tuttle, S. B. Desu, and P. K. Larsen, *MRS Symposia Proceedings No. 310* (Materials Research Society, Pittsburgh, 1993), p. 249.

¹²J. Zhang, R. A. Gardiner, P. S. Kirlin, R. W. Boerstler, and J. Steinbeck, *Appl. Phys. Lett.* **61**, 2884 (1992).

¹³S. Geller and V. B. Bala, *Acta Crystallogr.* **9**, 1019 (1956).

¹⁴Z. L. Wang and A. J. Shapiro, *Surf. Sci.* **328**, 141 (1995).

¹⁵Z. L. Wang and A. J. Shapiro, *Surf. Sci.* **328**, 159 (1995).

¹⁶H. L. Yakel, *Acta Crystallogr.* **8**, 394 (1955).

¹⁷F. S. Galasso, *Structure, Properties and Preparation of Perovskite-type Compounds* (Pergamon, New York, 1969), Chap. 1.

¹⁸J. M. Cowley, in *High Resolution Transmission Electron Microscopy and Associated Techniques*, edited by P. Buseck, J. Cowley, and L. Eyring (Oxford University Press, New York, 1989).

¹⁹G. H. Jonker and J. H. van Santen, *Physica* **19**, 120 (1953).

²⁰J. F. M. Cillessen, R. M. Wolf, and A. E. M. De Veirman, *Appl. Surf. Sci.* **69**, 212 (1993).

²¹C. Zener, *Phys. Rev.* **82**, 403 (1951).

²²P. W. Anderson and H. Hasegawa, *Phys. Rev.* **100**, 675 (1955).

²³P. G. de Gennes, *Phys. Rev.* **118**, 141 (1960).

²⁴G. A. Prinz, *Phys. Today* **XX** (April), 58 (1995).

²⁵S. Jin, M. McCormack, T. H. Tiefel, and R. Ramesh, *J. Appl. Phys.* **76**, 6929 (1994).

²⁶Z. L. Wang and J. Zhang, *Philos. Mag. A* **72**, 1513 (1995).